

Original Article

Cite this article: Lan Z, Wu S, Roberts NMW, Zhang S, Cao R, Wang H, and Yang Y (2022) Geochronological and geochemical constraints on the origin of highly $^{13}\text{C}_{\text{carb}}$ -depleted calcite in basal Ediacaran cap carbonate. *Geological Magazine* **159**: 1323–1334. <https://doi.org/10.1017/S001675682200019X>

Received: 30 November 2021

Revised: 9 February 2022

Accepted: 28 February 2022

First published online: 4 April 2022

Keywords:


cap carbonate; South China; calcite U–Pb geochronology; calcite REE; LA-ICP-MS

Author for correspondence:

Zhongwu Lan,

Email: lzw1981@126.com

Geochronological and geochemical constraints on the origin of highly $^{13}\text{C}_{\text{carb}}$ -depleted calcite in basal Ediacaran cap carbonate

Zhongwu Lan^{1,2,3} , Shitou Wu¹, Nick M. W. Roberts⁴, Shujing Zhang⁵, Rong Cao^{1,6}, Hao Wang¹ and Yueheng Yang¹

¹State Key Laboratory of Lithospheric Evolution, Institute of Geology and Geophysics, Chinese Academy of Sciences, Beijing 100029, China; ²State Key Laboratory of Palaeobiology and Stratigraphy, Nanjing Institute of Geology and Palaeontology, Chinese Academy of Science, Nanjing 210008, Jiangsu, China; ³State Key Laboratory of Geological Processes and Mineral Resources, China University of Geosciences, Wuhan 430074, Hubei, China; ⁴Geochronology and Tracers Facility, British Geological Survey, Keyworth, NG12 5GG, UK; ⁵Department of Geology, School of Natural Sciences, Trinity College Dublin, Dublin 2, Ireland and ⁶University of Chinese Academy of Sciences, Beijing 100049, China

Abstract

Ediacaran cap dolostone atop Marinoan glacial deposits contains complex sedimentary structures with extremely negative $\delta^{13}\text{C}_{\text{carb}}$ values in close association with oscillations in palaeoclimatic and oceanographic proxy records. However, the precise geological, geochronological and geochemical context of the cap dolostone is not clarified, which hampers us from correctly interpreting the extremely negative $\delta^{13}\text{C}_{\text{carb}}$ values and their causal relationships with the Snowball Earth hypothesis. In this study, we conducted detailed *in situ* geochronological and geochemical analyses on the calcite within the cap dolostone from the Ediacaran Doushantuo Formation in South China in order to define its formation and relationship to the Snowball Earth hypothesis. Petrographic observations show that formation of dolomite pre-dates precipitation of calcite and pyrite, which pre-dates quartz cementation in the basal cap carbonate. Calcite cement within the cap dolostone yielded a U–Pb age of $636.5 \pm 7.4/17.8$ Ma (2σ , MSWD = 1.6, $n = 36/40$), which is within uncertainty of a published dolomite U–Pb age of 632 ± 17 Ma (recalculated as $629.3 \pm 16.7/22.9$ Ma). These age constraints negate the possibility that the calcite cement was formed by late Ediacaran or Cambrian hydrothermal activity. The rare earth element distribution patterns suggest a dominant seawater origin overprinted by subsequent early Ediacaran hydrothermal activity. The combined age, petrographic and geochemical data suggest oxidization of methane clathrates in response to complicated interplay between eustasy and isostatic rebound and hydrothermal fluids.

1. Introduction

The globally distributed Marinoan cap dolostone overlying the Marinoan glaciogenic deposits represents a suite of unique sedimentary successions that continues to attract worldwide attention (Kennedy *et al.* 2001; Hoffman & Schrag, 2002; Jiang *et al.* 2003, 2006; Shields *et al.* 2007; Bao *et al.* 2008; Wang *et al.* 2008; Zhou *et al.* 2010, 2017; Bristow *et al.* 2011). Yet, the perplexing sedimentary structures and anomalously negative carbon isotope signals registered in the Marinoan cap dolostone make it difficult to explain the detailed sedimentological and petrographic context, although numerous geochemical and isotopic data have been intermittently reported. Specifically, the origin of calcite with extremely negative $\delta^{13}\text{C}$ values, and its petrographic and genetic relationships with paragenetic minerals and Marinoan deglaciation, remains disputed. Oxidization of methane was proposed to have offered excess CO_3^{2-} inducing carbonate precipitation and explained the observed extremely negative carbon isotope anomaly (Jiang *et al.* 2003; Kennedy *et al.* 2008; Wang *et al.* 2008), but whether such a process occurred during deposition/early diagenetic or later hydrothermal activity remains disputed (Zhou *et al.* 2010, 2017; Bristow *et al.* 2011). It follows that ascertaining the temporal sequence of calcite and paragenetic minerals and their formation mechanisms would contribute to our understanding of their causal relationships with the Snowball Earth hypothesis, as well as providing a sound interpretation of geochemical data.

Calcite has frequently been utilized in probing the timing and causal relationships of biological and environmental events recorded in carbonates by means of measuring radiogenic U–Pb and stable C–O isotopic systems and trace-element compositions (Wang *et al.* 2008; Bristow *et al.* 2011; Franchi *et al.* 2015; Kalliomäki *et al.* 2019; MacDonald *et al.* 2019; Roberts *et al.* 2020). This is because calcite commonly incorporates rare earth elements (REEs)

and uranium during its crystallization, making it a suitable host for REE analyses and a potential chronometer for U–Pb geochronology. Calcite REE compositions are used as key evidence to distinguish its origin, as variations in REE distribution patterns are suggestive of variations of circulating fluid chemistry. Specifically, calcite with low REE concentrations and a positive Eu anomaly commonly precipitates from hydrothermal fluids, whereas calcite with positive La and Gd anomalies, a superchondritic Y/Ho ratio and light REE (LREE) depletion commonly forms in normal seawater (Van Kranendonk *et al.* 2003; Franchi *et al.* 2015; Kalliomäki *et al.* 2019).

Owing to differential geochemical behaviour and the abundance of U and Pb in seawater (Ku *et al.* 1977; Shen & Boyle, 1987), marine carbonates are particularly suitable for U–Pb dating because of their commonly high U/Pb ratios (Rasbury *et al.* 2004). As such, calcite geochronology could potentially produce direct age constraints in various geoscience applications (Rasbury & Cole, 2009; Roberts *et al.* 2020). Laser ablation-inductively coupled plasma-mass spectrometry (LA-ICP-MS) has been demonstrated to be an effective tool for *in situ* calcite U–Pb dating and REE composition measurement because of rapid *in situ* spot analysis with adequate levels of precision (Li *et al.* 2014; Roberts & Walker, 2016; Coogan *et al.* 2016; Ring & Gerdes, 2016; Nuriel *et al.* 2017; Kalliomäki *et al.* 2019; MacDonald *et al.* 2019; Roberts *et al.* 2020; Wu *et al.* 2022). This paired approach proves robust in constraining the formation timing of calcite and fingerprinting the source of fluids and thus tracing fluid evolution processes. To this end, we carry out detailed REE and U–Pb isotope analyses combined with scanning electron microscope (SEM) and cathodoluminescence (CL) imaging techniques on calcite from the Marinoan cap dolostone at the Jiulongwan type section to decipher its genesis and timing of formation. The findings provide further constraints on our understanding of its relationship with the Snowball Earth hypothesis.

2. Geological setting and sampling information

The late Mesoproterozoic to earliest Neoproterozoic Jiangnan Orogeny resulted in the formation of the South China Block (SCB) by means of amalgamating the Yangtze Block to the northwest with the Cathaysia Block to the southeast, along the Jiangnan Orogen (Li *et al.* 2009). The SCB experienced a subsequent intra-continental rifting, and accommodated abundant well-preserved Neoproterozoic sedimentary successions in the Nanhua Basin: the largest Neoproterozoic basin in the SCB (Wang & Li, 2003). Such a suite of sedimentary successions is well exposed in the Hubei–Hunan–Guizhou–Guangxi regions of the Nanhua Basin. The Ediacaran Yangtze platform in South China developed on a Neoproterozoic rifted continental margin that is interpreted to have started along the southeastern side of the Yangtze Block at *c.* 800 Ma (Wang & Li, 2003; Jiang *et al.* 2007). The Ediacaran carbonate and siliciclastic rocks were assumed to have been accommodated in a passive margin setting (Jiang *et al.* 2003, 2007). Ediacaran sedimentary rocks in South China are composed of the fossiliferous Doushantuo and Dengying formations, which show a wide spatial occurrence around the Yangtze Block, preserving key biostratigraphic and chemostratigraphic records regarding the coevolution of life and environmental conditions (Fig. 1a, b; Lan *et al.* 2019 and references therein).

Previous sedimentological research suggests deposition of the Doushantuo Formation in two stages. The first stage witnessed deposition of the couplet of cap carbonate and overlying black

shale of the lower Doushantuo Formation in an open shelf/ramp depositional environment, whereas the second stage is typical of a rimmed carbonate shelf with a shelf-margin barrier separating the intra-shelf lagoon from open ocean settings (Jiang *et al.* 2011). The Yangtze Gorges area accommodated the most complete and continuous outcrops of the Doushantuo Formation exposed at the Jiulongwan, Huajipo and other sections (Jiang *et al.* 2011). The Doushantuo Formation is best exposed at the intra-shelf basin Jiulongwan section (Jiang *et al.* 2011). Therein, the Doushantuo Formation has a conformable contact with the underlying Nantuo Formation (Fig. 2a, b), and is composed of *c.* 160 m thick mixed shale and carbonate. The Nantuo Formation is dominated by glaciogenic greenish diamictite with minor sandstone beds correlative with the late Cryogenian ‘Marinoan glaciation’ (Lang *et al.* 2018). The Doushantuo Formation is dividable into, in ascending order, Member 1 composed of cap dolostone, Member 2 dominated by black shale, Member 3 dominated by dolostone and Member 4 composed exclusively of black shale (with carbonate concretions). Regionally traceable cap carbonates in the basal Doushantuo Formation show anomalously negative $^{13}\text{C}_{\text{carb}}$ excursions and intriguing sedimentary structures such as stromatolite-like cavities, botryoidal cemented breccias, layer-parallel sheet cracks and tepee-like positive reliefs (Jiang *et al.* 2003; Wang *et al.* 2008), which has led to them receiving the most intensive investigation among the worldwide Neoproterozoic successions.

A time interval between *c.* 635 Ma and 550 Ma was constrained for the depositional age of the Doushantuo Formation exposed at the Jiulongwan and Jijiawan sections by means of thermal ionization mass spectrometry (TIMS) U–Pb dating of zircon grains from two interbedded tuff beds around the basal Doushantuo Formation and near the Doushantuo–Dengying Formation boundary (Condon *et al.* 2005; Yang *et al.* 2021; Fig. 1c). The cap dolostone at the Jiulongwan section is mainly composed of three components; they are a disrupted poorly stratified limestone/dolostone layer, laminated limestone/dolostone displaying tepee-like structures, and laminated silty limestone/dolostone (Jiang *et al.* 2003; Fig. 1c). Multiple generations of botryoidal cements filled in irregular cavities possibly formed by vertical extension of micritic crusts (Jiang *et al.* 2003; Fig. 2c, d). The tepee-like structures display positive relief and are made up of laminated micrite and dolomiticite, which bear layer-parallel sheet cracks surrounding the host carbonate (Jiang *et al.* 2003). These characteristics suggest they were probably formed by means of layer-parallel compression and vertical extension (*c.f.* Hoffman & Macdonald, 2010). Sample 1-2 is a fresh grape-structured dolostone collected from the disrupted dolostone layer that is *c.* 130 cm below the *c.* 635 Ma tuff bed; it is mainly composed of dolomite and calcite that are quartz cemented (Fig. 2e).

3. Analytical methods

In this study, both imaging analysis and *in situ* element and isotope analyses were conducted in order to reveal the formation timing and origin of calcite and its relationship with a syngenetic mineral assemblage in cap dolostone, as detailed below.

3.a. Imaging analysis

Polished thin-sections were prepared for petrographic observations and selection of spots for *in situ* mineral chemistry and calcite geochronology. A Nikon Eclipse E800 microscope equipped with a

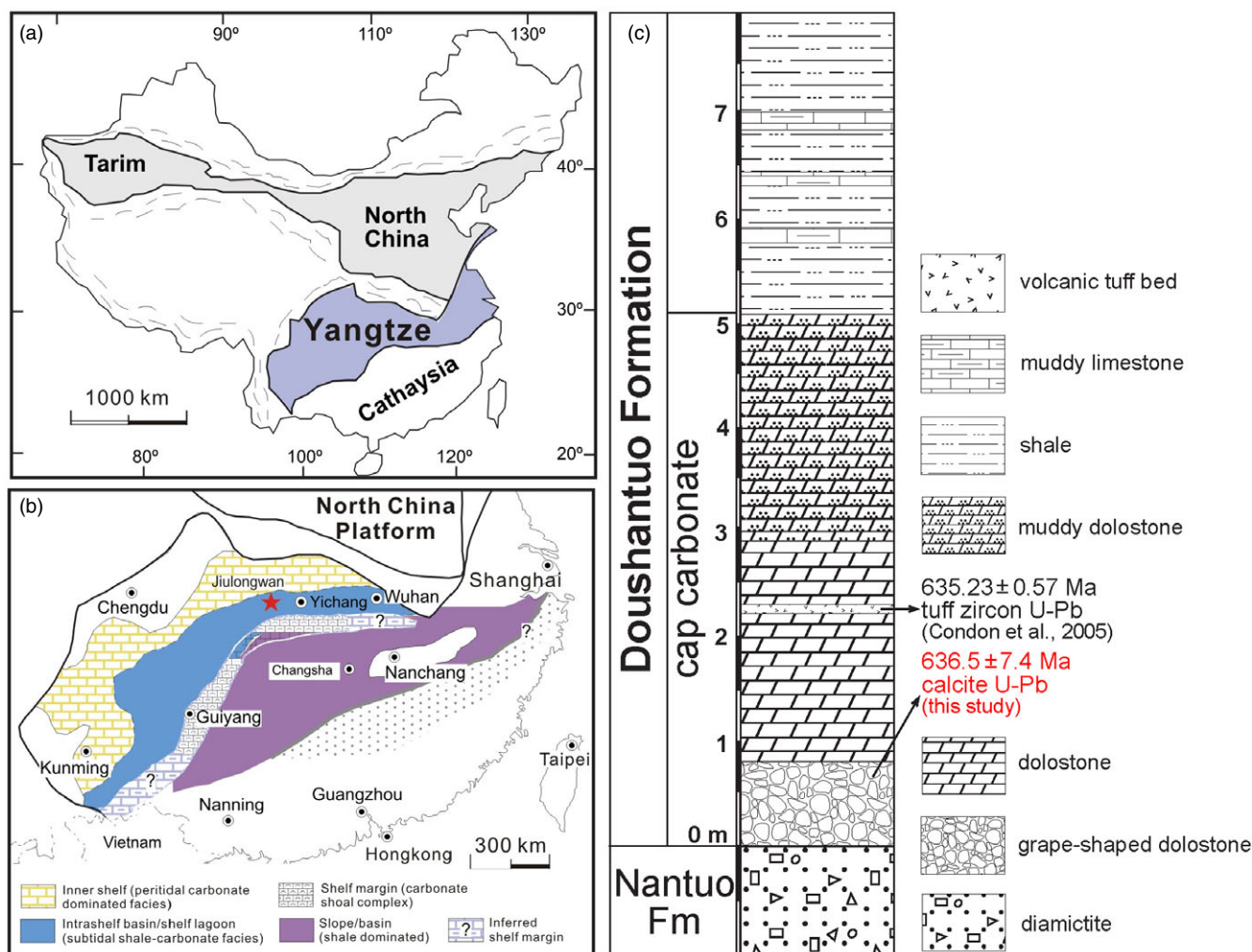


Fig. 1. (Colour online) (a) Geological map of China with the Yangtze platform highlighted in purple colour. (b) Reconstructed Ediacaran depositional environments on the Yangtze platform (Jiang *et al.* 2011). Red star marks the study location. (c) Stratigraphic column showing the sampling horizon in the cap dolostone of Doushantuo Formation.

Nikon DS-Fi 1 camera and Zeiss 1555 VP-FESEM at the State Key Laboratory of Lithospheric Evolution, Institute of Geology and Geophysics, Chinese Academy of Sciences (SKLLE, IGGCAS) were utilized to detect textural relationships for syngenetic minerals. The SEM was specifically manipulated under backscattered electron mode to get an optimal resolution at 50–650 \times magnification. It was adjusted to an optimal working distance of 6–8 mm and a voltage of 10 kV. In order to obtain CL images of carbonates, a cold CL microscope at the Key Lab of Petroleum Resources at IGGCAS was utilized with a beam voltage of 16 kV, a current of 325 μA and a beam diameter of 4 mm.

3.b. Calcite REE composition analysis

Trace-element contents of calcite were determined by LA-ICP-MS employing an Element XR HR-ICP-MS instrument (Thermo Fisher Scientific, USA) coupled to a 193 nm ArF excimer laser system (Geolas HD, Lambda Physik, Göttingen, Germany) at SKLLE, IGGCAS. The approach is similar to those outlined in Wu *et al.* (2018) with isotopes measured using a peak-hopping mode with a laser beam diameter of *c.* 44 μm , a repetition rate of 5 Hz and a laser energy density of $\sim 3.0 \text{ J cm}^{-2}$. Helium was employed as the ablation gas to improve the transporting efficiency

of ablated aerosols. ARM-3 (Wu *et al.* 2019) reference glass was used as a calibration reference material, and BIR was analysed for data quality control. Calcium (^{40}Ca) was used as an internal standard. The resulting data were reduced using the GLITTER program (Griffin *et al.* 2008). For most trace elements ($>0.05 \mu\text{g/g}$), the accuracy is better than $\pm 10\%$ with analytical precision (1 RSD) of $\pm 10\%$.

3.c. Calcite U-Pb dating

Detailed procedures of the instrumentation and analytical protocol for calcite U-Pb dating are given in Wu *et al.* (2022) and are only briefly summarized herein. A Photo Machine Analyst G2 laser ablation system (Teledyne CETAC, Omaha, USA) coupled to an Element XR (Thermo Fisher Scientific, Bremen, Germany) was adopted to carry out *in situ* calcite U-Pb dating on polished thin-sections using LA-ICP-MS at SKLLE, IGGCAS. A high-capacity vacuum pump was used to make the high-performance Jet sample cone work efficiently. The guard electrode was used to improve sensitivity (Wu *et al.* 2020a,b), while a T junction was adopted to add N_2 into the Ar sample gas flow behind the ablation cell.

A blind spot analysis was conducted using a laser beam of 80 μm to screen for high uranium regions for subsequent detailed



Fig. 2. (Colour online) Field and petrographic photos showing the cap dolostone of the Doushantuo Formation at the Jiulongwan section, Three Gorges area, South China. (a) The boundary between the Nantuo and Doushantuo formations. (b) Cap dolostone of the Doushantuo Formation. (c, d) Cap dolostone with botryoidal structures. Hammers in (c) and (d) are c. 35 cm long. (e) Merged reflected light images showing the petrography of grape-structured dolostone that is dominated by dolomite and calcite that are quartz cemented. D – dolomite; C – calcite; Q – quartz. The white dotted circles indicate laser analysis spots in calcite.

in situ U–Pb spot dating analysis. An automated mode in sequences of 60 to 80 spot analyses was used to acquire raw data. Each spot analysis is composed of 8 s of background acquisition followed by 25 s of sample ablation and 30 s washout. A peak jumping mode with a total integration time of 0.30 s to produce 130 mass scans was adopted to detect the signals of ^{202}Hg , $^{204}(\text{Hg} + \text{Pb})$, ^{206}Pb , ^{207}Pb , ^{208}Pb , ^{232}Th and ^{238}U during the data acquisition. In this study, a total of four reference materials (RMs) were used including two calcite U–Pb reference materials for calibration of U/Pb ratios and validation of the results (WC-1 and Duff Brown Tank; Hill *et al.* 2016; Roberts *et al.* 2017) and two glass reference materials for calibration of Pb/Pb ratios and

drift correction (ARM-3 and NIST SRM 614; Woodhead & Hergt, 2001; Wu *et al.* 2021). Two analyses of glass NIST SRM 614 and ARM-3 in combination with three analyses of WC-1 were analysed bracketing every ten analyses of unknown samples. The Duff Brown Tank (64.04 ± 0.67 Ma; Hill *et al.* 2016) was treated as an unknown sample to monitor data accuracy.

A total of 40 spot analyses were carried out on sample 1-2. The data reduction method follows those described recently by Wu *et al.* (2022), and uses the premise of calibrating against a material with known age but heterogeneous composition as per Roberts *et al.* (2017) and Chew *et al.* (2014). The Iolite 3.7 data reduction software and the VizualAge data reduction scheme were used to

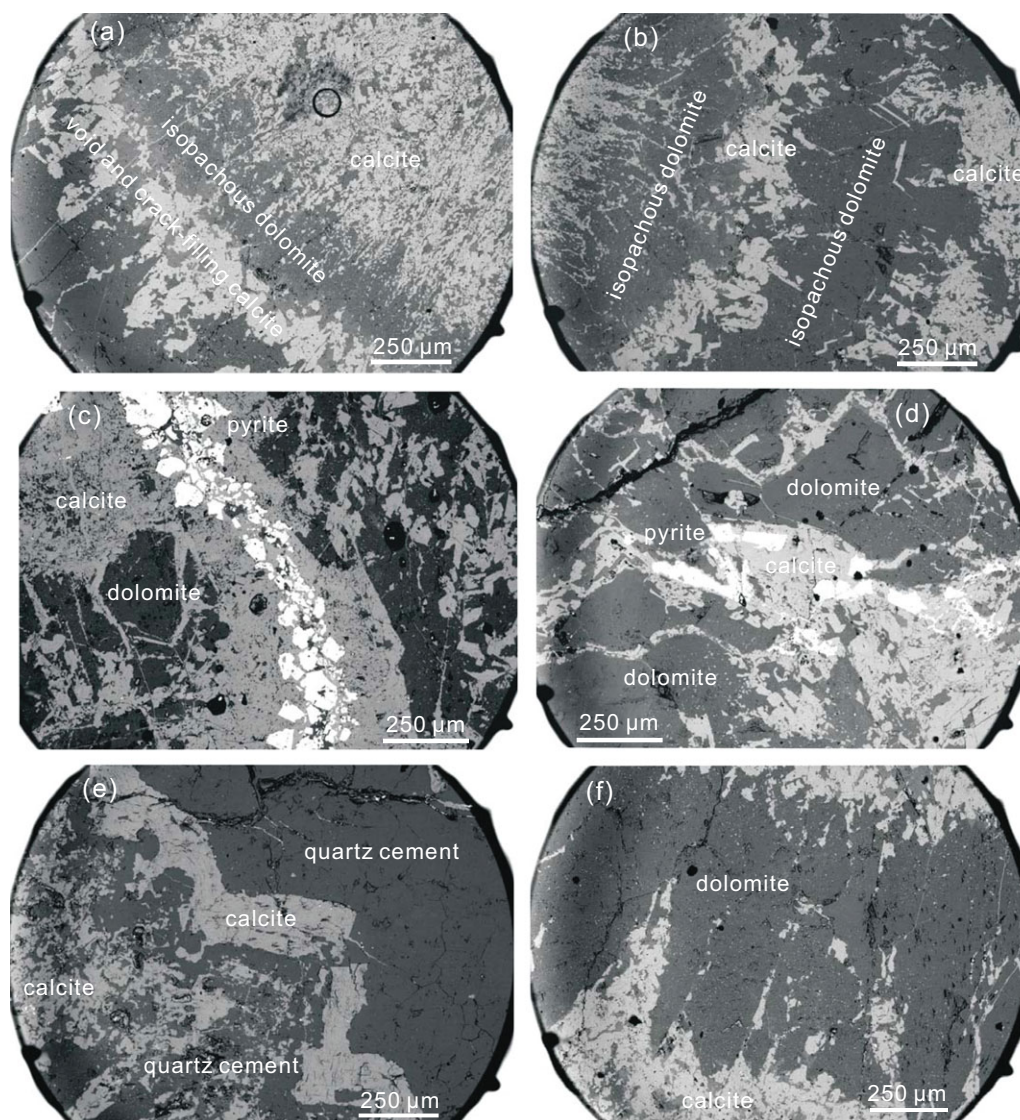


Fig. 3. Backscattered electron (BSE) images of cap dolostone showing paragenetic mineral assemblage. Initial dolostone deposition was followed by exposure and karstification due to isostatic rebound, forming voids and cracks that were subsequently filled by multidirectional straight or flexured pyrite and calcite cements/veins (a–e), which were then quartz cemented (e). The dolostone is mainly composed of isopachous dolomite. Black circle in (a) represents laser analysis spot.

reduce the raw data (time-resolved intensities) from the ICP-MS (Paton *et al.* 2011; Petrus & Kamber, 2012). Correction of instrument drift and calculation of isotope ratios of $^{207}\text{Pb}/^{206}\text{Pb}$ is accomplished by linear fit of ARM-3. The recommended value of $^{207}\text{Pb}/^{206}\text{Pb}$ is taken from Wu *et al.* (2021). NIST SRM 614 is used for the accuracy monitoring of $^{207}\text{Pb}/^{206}\text{Pb}$. Ten analyses of NIST SRM 614 yielded a mean of 0.8684 ± 0.0093 (2s), which is in agreement with the recommended value of 0.8710 ± 0.0004 (2s) (Baker *et al.* 2004). The downhole fractionation profile from ARM-3 glasses was used to calibrate the laser induced elemental fractionations of WC-1 and other samples (Wu *et al.* 2022). After the initial correction, WC-1 was used for further calibration of matrix-induced mass bias in $^{238}\text{U}/^{206}\text{Pb}$ ratios between RMs and unknown samples, which was accomplished in Microsoft Excel. The uncertainty propagation of LA-ICP-MS calcite geochronology is a modified approach based upon Horstwood *et al.* (2016), wherein the final age is quoted without and with systematic uncertainties, as $\pm \alpha/\beta$, respectively.

4. Results

4.a. Petrography of the studied samples

Field outcrops show that botryoidal structures and cavities widely occur in the basal cap dolostone, which is poorly stratified (Fig. 2a, c, d). Initial deposition of cap dolostone was followed by subsequent uplifting because of isostatic rebound, during which the cap dolostone experienced karstic dissolution in shallow marine to marginal depositional settings in South China, forming abundant cavities (Zhou *et al.* 2010). The botryoidal structures probably formed during a subsequent transgression, which induced a series of mineral precipitation within these cavities. The botryoidal structures not only encrust the bed surface but also the surface of cavities, with a thickness of 1–5 cm (Fig. 2c, d). Microscopic observations show the dolostone sample is mainly composed of dolomite, calcite, pyrite with minor barite and iron oxide (Figs 3, 4, 5). In most cases, calcite occurs as void and crack fillings among isopachous (about 200–500 μm thick) dolomite

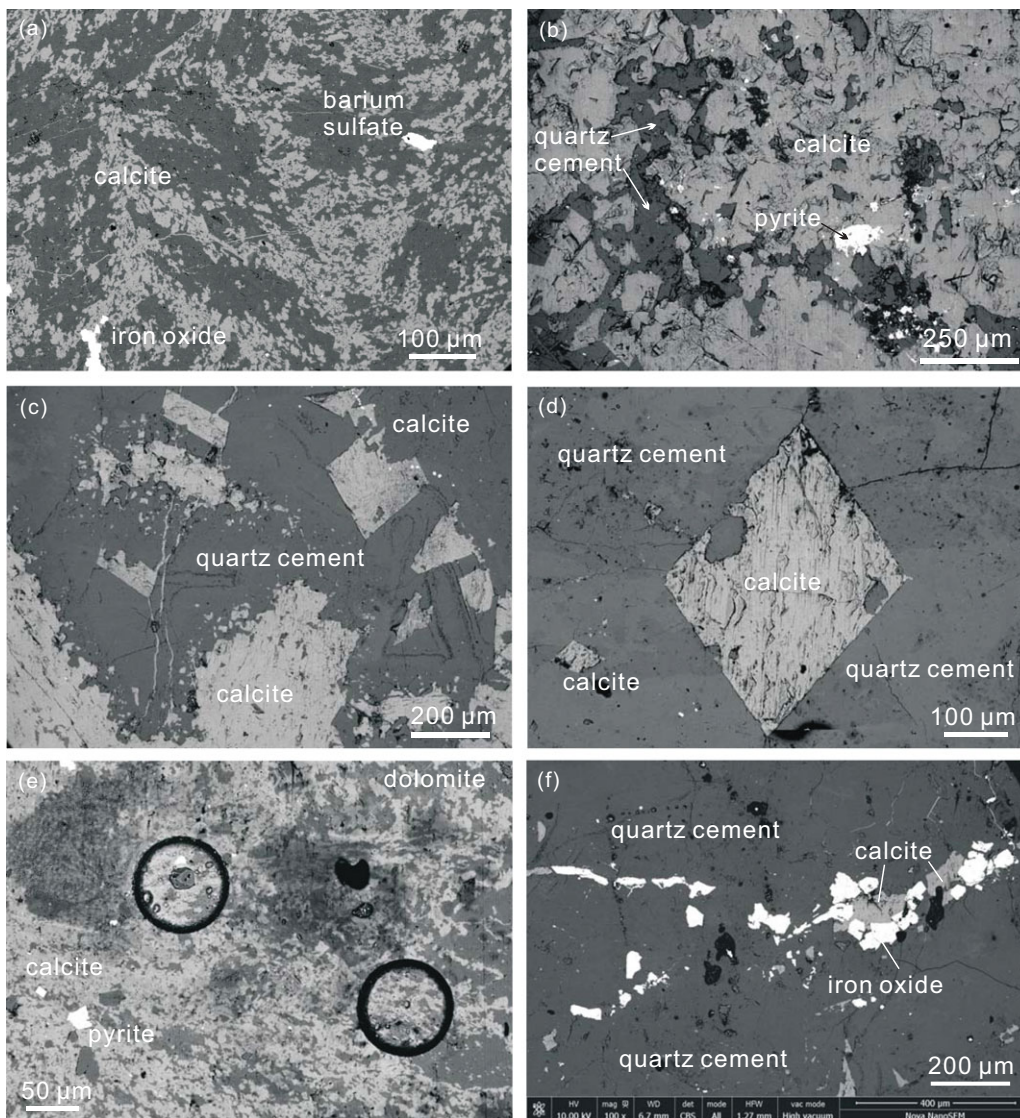


Fig. 4. Backscattered electron (BSE) images of cap dolostone showing paragenetic mineral assemblage. Various kinds of calcite cements/grains, pyrite or iron oxide, and barite filled in the cracks and cavities in dolostone that was formed via karstification, and was then quartz cemented. Black circles in (e) represent laser analysis spots.

(Fig. 3a, b, f). Most of the crack fillings display tapering ends. Finer cracks locally occur abundantly as meshworks (Fig. 3b, c). In some places, calcite veins, 30–500 μm thick, co-occur with pyrite (up to 250 μm) as vein fillings extending in various directions (Fig. 3c, d). Some calcite occurs as flexured isopachous veins, about 250 μm thick in quartz cements (recrystallized chalcedony and micro-quartz) (Fig. 3e). Aside from these phenomena, fibrous/amorphous calcite cements are seen to co-occur with fine barite and iron oxides/pyrite of 30–100 μm within dolomites (Fig. 4a, e). Amorphous quartz cement widely occurs filling the pore spaces of calcite cement (Fig. 4b) or entombing euhedral calcite or iron oxide grains (Fig. 4c, d). The euhedral calcite grains have a size range of 50–350 μm , some of which bear porous margins infilled by quartz cements (e.g. Fig. 4d). The iron oxides, 50–150 μm in size, are intimately associated with calcite (Fig. 4f). Under CL, calcite cements display a bright orange colour, whereas dolomite crystals show a blue colour (Fig. 5).

4.b. Calcite REE composition

LA-ICP-MS calcite REE compositions are tabulated in online Supplementary Material Table S1. Overall, the calcite shows a bell-shaped distribution pattern. They are characterized by positive La and Y anomalies, and high Y/Ho ratios (39–61 with an average of 50) (Fig. 6). Except for three points that have Y/Ho ratios of 39–41, the other 20 points all have Y/Ho ratios of >44. A prominent positive Gd anomaly is also present with δGd in the range of 1.1–1.96. Eu is dominated by positive anomalies ($\delta\text{Eu} = 1.02\text{--}1.38$) with minor slightly negative anomalies ($\delta\text{Eu} = 0.79\text{--}0.96$). $\text{Pr}_{\text{SN}}/\text{Yb}_{\text{SN}}$ ratios vary from 0.3 to 3.0 with an average of 0.9.

4.c. Calcite U-Pb geochronology

LA-ICP-MS calcite U-Pb dating results are tabulated in online Supplementary Material Table S2. A total of 185 spot analyses (over one month) were conducted for Duff Brown Tank, which

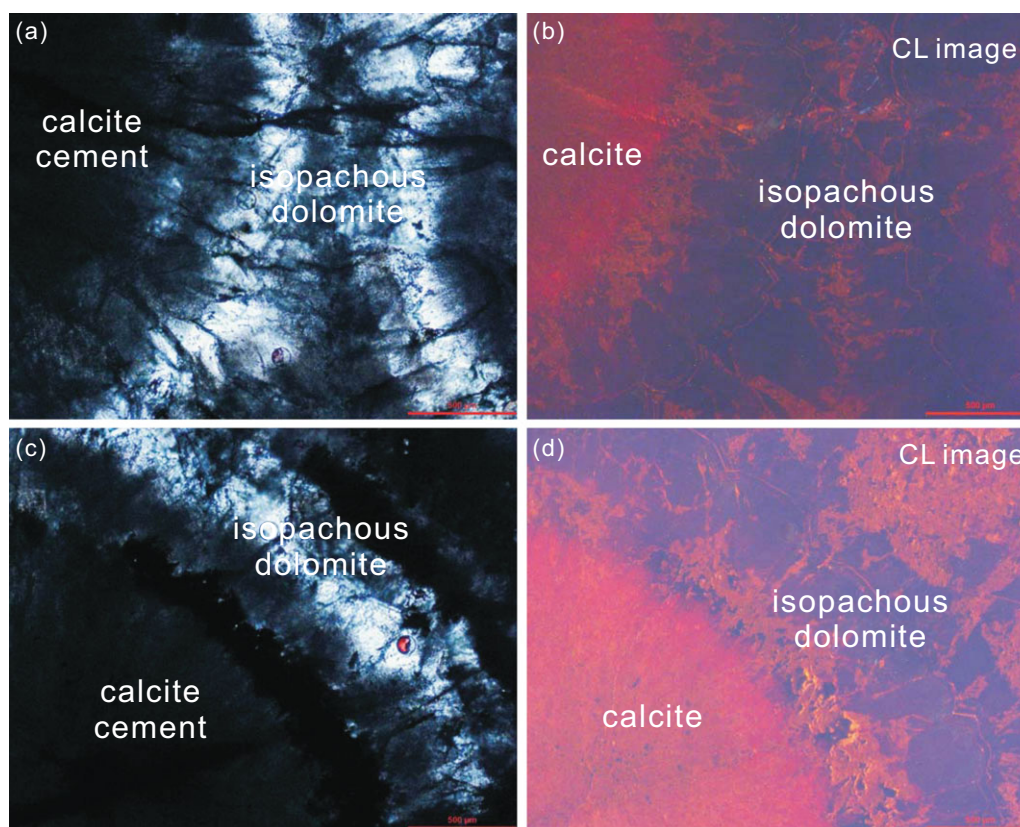


Fig. 5. (Colour online) Cathodoluminescence (CL) photomicrographs for sample 1-2 used as reference for choosing laser spots. (a) and (c) are reflected light images, whereas (b) and (d) are their corresponding CL images. Calcite cements show a distinct bright orange colour, which is in sharp contrast to the isopachous dolomite crystals which show a blue colour.

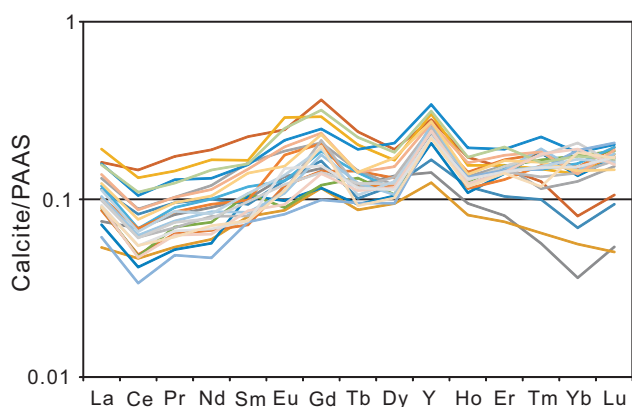


Fig. 6. (Colour online) Calcite rare earth element (REE) post-Archaean Australian shale (PAAS) normalized plot.

yielded a pooled age of 62.44 ± 0.91 Ma (MSWD = 7.2) (Fig. 7a), whereas 10 spot analyses during the analytical session for sample 1-2 yielded an intercept age of 62.63 ± 2.80 Ma (MSWD = 1.7). Both of these two ages are within uncertainty of the published isotope dilution age (Hill *et al.* 2016). These results suggest the long-term reproducibility across different analytical sessions is no larger than the limiting 2.5% age uncertainty of the WC-1 reference material. During analysis, only calcite cements with smooth surfaces were chosen for U–Pb geochronology. A total of 40 spot analyses were conducted on the calcite cements of sample 1-2. Four

spots fall to the right of a distinct regression in Tera–Wasserburg space, and thus were removed; they may reflect a slight amount of open-system behaviour, i.e. U mobility, in the sampled region. The remaining 36 spots yield a lower intercept age of 636.5 ± 7.4 Ma (2σ , MSWD = 1.6, $n = 36/40$) (Fig. 7b). After propagation of decay constant and reference material (WC-1) uncertainties, the final age uncertainty that is required for age comparison is 17.8 Ma. As such, $636.5 \pm 7.4/17.8$ Ma is interpreted as the depositional age of the sampling horizon.

5. Discussion

5.a. Constraints on the cap dolostone

The complex sedimentary structures and anomalously negative carbon isotope signals registered in the cap dolostone are deemed to be associated with methane release induced by destabilization of low-latitude permafrost clathrates, which have aided in triggering the Marinoan deglaciation and subsequent flooding of continental shelves (Kennedy *et al.* 2001, 2008; Jiang *et al.* 2003). Authigenic calcite cements with extremely negative $\delta^{13}\text{C}_{\text{carb}}$ values (< -45 ‰) are the critical evidence in favour of the hypothesis that oxidization of methane hydrate offered excess CO_3^{2-} and induced the precipitation of cap dolostone (Jiang *et al.* 2003; Kennedy *et al.* 2008; Wang *et al.* 2008). It remains disputed, however, whether such a process occurred during deposition or early diagenesis, or during later hydrothermal activity (Zhou *et al.* 2010, 2017; Bristow *et al.* 2011). Our petrographic, geochemical and geochronological data demonstrate that these calcite cements were either originally

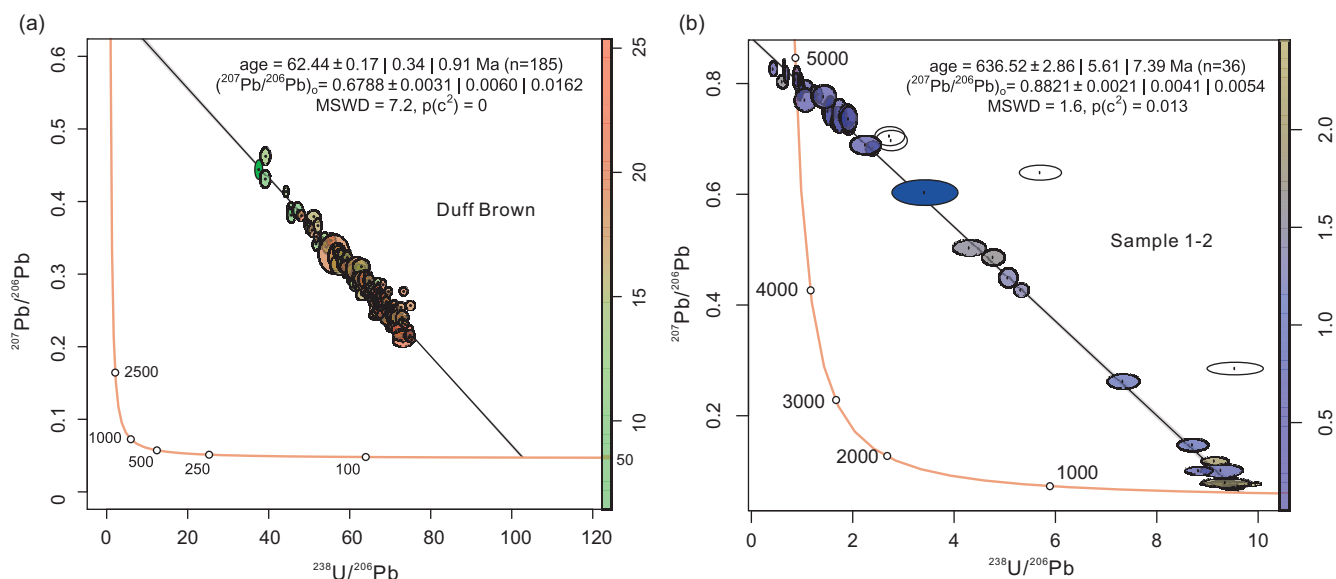


Fig. 7. (Colour online) Tera-Wasserburg Concordia plots (using IsoplotR; Vermeesch, 2018) of (a) reference material Duff Brown Tank and (b) sample 1-2. The upper intercepts define common Pb compositions, whereas the lower intercepts define dates that are quoted as $\pm \alpha/\beta$; see text for explanation.

precipitated in normal seawater and subsequently overprinted by early Ediacaran hydrothermal activities or were purely formed in early Ediacaran hydrothermal fluids, as detailed below.

It is commonly accepted that the shale-normalized REE + Y pattern of modern seawater is characterized by strong LREE depletion ($Pr_{SN}/Yb_{SN} = 0.2\text{--}0.4$), positive La and Gd ($Gd/Gd^* = 1.05\text{--}1.30$) and negative Ce anomalies, and superchondritic Y/Ho ratios ranging from 44 to 74 (Franchi *et al.* 2015 and references therein). The post-Archaeon Australian shale (PAAS)-normalized REE distribution patterns for the calcite cements in the cap dolostone display an overall slightly LREE depletion ($Pr_{SN}/Yb_{SN} = 0.3$ to 3.0), positive La and Gd anomalies ($Gd/Gd^* = 1.10\text{--}1.96$) and negative Ce anomalies, and high Y/Ho ratios (most of which are >44 with an average of 50), which are typical of precipitation from normal marine seawater. Y and Ho have the same charge and similar ionic radius, with the latter removed from seawater much faster than the former because of differential complexation behaviour (Nozaki *et al.* 1997). This explains why the calcite has high Y/Ho ratios. Ce is present as Ce(IV) in oxygenated environments that can be readily incorporated into Fe-oxyhydroxides (Derry & Jacobsen, 1990), resulting in a negative Ce anomaly in marine precipitate. As such, Ce anomalies can be used to infer the seawater redox state; a negative Ce anomaly indicates an oxygenated oceanic condition, whereas a positive Ce anomaly reflects an anoxic depositional environment (Hu *et al.* 2014; Franchi *et al.* 2015). The uniform negative Ce anomalies in our calcites are consistent with an oxygenated oceanic condition.

Insofar as barite is cogenetic with dolomite, calcite, pyrite/Fe-oxide and quartz in the basal Doushantuo Formation at the Jiulongwan section, a seawater origin also receives support from Ba-isotopes of barite ($BaSO_4$) in the Jiulongwan and other basal cap dolostone sections in South China (Crockford *et al.* 2019), which have nearly invariable isotope compositions of $\leq 0.1\text{‰}$ that are within the range of modern pelagic barite and barites in worldwide Marinoan cap dolostones. This is in sharp contrast to modern cold-seep barites, which have variable Ba-isotope compositions of $\leq 0.9\text{‰}$ (Crockford *et al.* 2019). Whereas the Ba-isotopes suggest a

well-mixed residual snowball brine for the source of Ba, $\Delta^{17}O$ anomalies of atmospheric origin recorded in the same barites suggest a runoff origin for the sulfate. Redox reaction may have driven barite precipitation in the context of mixing of anoxic brine with meteoric ice meltwater (Bao *et al.* 2008; Zhou *et al.* 2010).

On the other hand, REE patterns with positive Eu and negative Ce anomalies are suggestive of mixing of hydrothermal solutions with seawater at unknown dilution ratios (Franchi *et al.* 2015). Hydrothermal solutions are commonly enriched in LREEs and Eu because of breakdown of plagioclase; thus hydrothermal influence tends to induce LREE enrichment and positive Eu anomalies (e.g. Michard, 1989; Van Kranendonk *et al.* 2003). Almost half of our REE analyses show positive Eu and negative Ce anomalies, which, coupled with less distinctive LREE depletion patterns, can be interpreted to have resulted from a hydrothermal overprint. A hydrothermal overprint on the seawater composition is also demonstrated by the non-linear correlation between Y/Ho and La in our calcite cements, which are characterized by La excess (c.f. Kamber & Webb, 2001; Franchi *et al.* 2015), and commonly high Mn contents (7500–15 000 ppm) that are frequently recorded in typical hydrothermal calcite (Kalliomäki *et al.* 2019).

A hydrothermal influence also receives support from clumped isotope (Δ_{47}) analyses of calcite, fluid inclusion analyses of quartz cements and alteration of trioctahedral clays into chlorite (Bristow *et al.* 2011; Derkowski *et al.* 2013; Zhou *et al.* 2017). On the basis of clumped isotope (Δ_{47}) analyses, Bristow *et al.* (2011) found these calcite cements formed under a high-temperature regime ($T > 400\text{ °C}$) and thus interpreted them as thermogenic methane oxidation products by means of hydrothermal activity during early Ediacaran or even Cambrian time (Bristow *et al.* 2011). Meanwhile, fluid inclusion analyses in quartz cements produced homogenization temperatures of c. 160–220 °C with both high salinity (18.0–20.8 wt % NaCl equiv.) and low-salinity (6.3–8.3 wt % NaCl equiv.) end-members, which are suggestive of mixing of high- and low-salinity hydrothermal fluids (Zhou *et al.* 2017). Alteration of saponite into chlorite via corrensitite increased from lower in Member 2 to the cap dolostone, which is commensurate with a decrease of $\delta^{18}O$ and increase of

δD in trioctahedral clays and is interpreted to have resulted from hydrothermal fluid activity in the underlying Nantuo Formation and cap dolostone (Derkowski *et al.* 2013).

Petrographic observations allow identification of three sequences of depositional/cementation events. Dolomite was first precipitated, followed by the formation of calcite cements/minerals, pyrite/iron oxide and barite, which subsequently experienced quartz cementation (Figs 3, 4). Note that barite only occasionally occurs as finer microscopic grains in association with calcite and dolomite in our samples, whereas abundant macroscopic barite coating dolomites is present at shallow-platform facies sections in South China and NW Africa (Shields *et al.* 2007; Zhou *et al.* 2010). Such mineral assemblages could suggest multiple stages of cavity/crack filling in response to a complicated interplay between eustasy and isostatic rebound and hydrothermal solutions (Shields *et al.* 2007; Zhou *et al.* 2010, 2017). Dolomite was initially precipitated during glacier retreat and relative sea-level changes, and was subsequently uplifted and exposed as a result of isostatic rebound. This prompted the dolomite to experience a period of karstic dissolution followed by sequential calcite/pyrite/iron oxide/barite precipitation and quartz cementation. The wide occurrence of quartz cementation may suggest precipitation from silica-rich hydrothermal fluids (Zhou *et al.* 2017), which was compounded by intense silicate weathering of glacial loess during the Marinoan Snowball Earth deglaciation (Penman & Rooney, 2019).

How long calcite precipitation postdates the initial deposition of dolomite remains unclear. Gan *et al.* (2021) documented a LA-ICP-MS U–Pb age of 632 ± 17 Ma from the isopachous dolomite within the cap dolostone, which we recalculate as $629.3 \pm 16.7/22.9$ Ma, using IsoplotR to directly compare with our own date. This published date is within uncertainty consistent with the calcite U–Pb age of 636.5 ± 17.8 Ma in this study. Despite relatively large analytical uncertainties, these U–Pb ages deny a broad time interval between the dolomite and calcite precipitation, which means the latter should have been influenced by hydrothermal fluids associated with the early Ediacaran but not Cambrian volcanism, as previously assumed (Bristow *et al.* 2011). Derkowski *et al.* (2013) reported illite K–Ar ages of *c.* 430 Ma from Member 4 shale and *c.* 325 Ma from Member 2 K-bentonite at the Jiuqunao section, which is *c.* 25 km from the Jiulongwan section. These dates are best explained as Ar diffusion due to the effect of resetting of the K–Ar isotope system at 430–325 Ma. Instead, these earliest periods of calcite cementation possibly ascribe to early stage fluid activities in response to eustasy and isostatic rebound not exceeding 1.6 Myrs (Shields *et al.* 2007; Zhou *et al.* 2010), which was subsequently overprinted by *c.* 632 Ma hydrothermal fluid activity (Bristow *et al.* 2011).

Cui *et al.* (2019) specifically measured the C-isotope data of calcite cements within the basal cap dolostone, which reveals low $\delta^{13}\text{C}_{\text{carb}}$ values (down to -53.8 ‰) in multiple generations of vug-filling calcite cement surrounding the pre-existing dolomite crystals with positive $\delta^{13}\text{C}_{\text{carb}}$ values as high as $+6.3$ ‰. Such isotopic signatures occur in multiple sections in South China, including the Jiulongwan section from which samples were collected in this study. The commonly low $\delta^{13}\text{C}_{\text{carb}}$ values mean these calcite cements should have a common origin, i.e. precipitation in early Ediacaran seawater and subsequently overprinted by early Ediacaran, but not late Ediacaran or Cambrian, hydrothermal activity. These calcite cements should have formed within <3 Myr considering the interbedded tuff zircon TIMS U–Pb ages of *c.* 635 Ma and *c.* 632 Ma within the basal and lower cap dolostone.

Such a time interval can be negligible considering the analytical errors (*c.* 7 Myr) of our calcite U–Pb age.

In this regard, both anoxic oxidation of methane (Shields *et al.* 2007; Zhou *et al.* 2010) and thermogenic methane oxidation (Bristow *et al.* 2011; Zhou *et al.* 2017) could have occurred to account for the calcite + pyrite + barite + iron oxide assemblage and particularly anomalously negative $\delta^{13}\text{C}_{\text{carb}}$ values recorded in the cap dolostone. In the former case, precipitation of calcite with extremely negative $^{13}\text{C}_{\text{carb}}$ values would be nearly synchronous with deposition of cap dolostone, which means deglaciation was related to methane release into the atmosphere by means of destabilization of clathrates (Jiang *et al.* 2003; Kennedy *et al.* 2008; Wang *et al.* 2008). In the latter case, precipitation of calcite with extremely negative $^{13}\text{C}_{\text{carb}}$ values should postdate the initial deposition of cap dolostone to a time interval of *c.* 3 Myr, which means thermogenic methane oxidation would have occurred much later in the cap dolostone. In this scenario, deglaciation would be unrelated to methane release into the atmosphere by means of destabilization of clathrates (Shields *et al.* 2007; Zhou *et al.* 2010).

5.b. Reliability of calcite U–Pb geochronology for Precambrian application

A published tuff zircon TIMS U–Pb age from the lower cap carbonate of the Doushantuo Formation provides a direct test of our calcite laser U–Pb age. A tuff bed *c.* 230 cm above the base of the cap carbonate of the Doushantuo Formation yielded a zircon TIMS U–Pb age of 635.23 ± 0.57 Ma (MSWD = 0.55) (Condon *et al.* 2005). Our results from the sampling horizon, which is *c.* 130 cm from the dated tuff bed, produce a calcite U–Pb age of 636.5 ± 17.8 Ma. These ages overlap within uncertainty, with only a 0.2 % offset, indicating that the calcite U–Pb age is a robust estimate of the timing of sedimentation within the quoted analytical uncertainty. Also, our calcite U–Pb age of 636.5 ± 17.8 Ma is within uncertainty of the dolomite U–Pb age of 632 ± 17 Ma (Gan *et al.* 2021), again indicating its robustness for age estimation. LA-ICP-MS U–Pb dating of carbonates has been applied to material with ages ranging from the Mesoproterozoic to Quaternary, but mostly to the Mesozoic to Cenozoic (see Roberts *et al.* 2020). Because of high ratios of common to radiogenic lead, most older dates reported from Precambrian to Cambrian carbonates (Liivamägi *et al.* 2018, 2021; Meinhold *et al.* 2020) are rather imprecise (e.g. 5–12 % uncertainties 2σ). Along with the dolomite U–Pb age of 632 ± 17 Ma reported by Gan *et al.* (2021), and the recently reported 1010 ± 36 Ma age from an older sedimentary sequence in South China (Lan *et al.* 2022), our result is one of the most precise Precambrian dates obtained so far using the LA-ICP-MS method for U–Pb carbonate geochronology. These studies highlight the practicality of the LA-ICP-MS method and demonstrate the advantages of using an *in situ* technique, which namely, are the ability to make use of the heterogeneous distribution of U and Pb within calcite, in the measurement of a large spread in U–Pb ratios from a single sample along with the avoidance of altered or mixed domains (Roberts *et al.* 2020). These advantages are difficult to achieve with dissolution and dilution-based methods owing to the averaging effect of coarser sampling. The success of this study gives us confidence that reliable U–Pb carbonate ages for other Precambrian successions can be obtained. Given that Precambrian carbonate rocks contain key information regarding the coevolution of life and environment, laser ablation U–Pb dating of carbonate minerals has great potential for providing important age constraints on biological and

environmental events such as the Great Oxygenation Event and the Bitter Springs Anomaly.

6. Summary and conclusions

Based on an integrated calcite LA-ICP-MS U–Pb dating and REE measurement combined with SEM and CL imaging analyses, the following conclusions can be drawn:

- (1) Calcite cements widely occur as irregular cavity/crack fillings in the cap dolostone of the Doushantuo Formation at the Jiulongwan section, South China, where they co-occur with pyrite, iron oxide and barite.
- (2) Petrographic observations show calcite (including cements and single finer grains) and pyrite postdate the initial deposition of dolomite but pre-date quartz cements. Some calcite cements show a bright orange CL colour, probably indicating hydrothermal overprint.
- (3) Calcites show positive La and Gd anomalies ($\delta\text{Gd} = 1.1\text{--}1.96$), a negative Ce anomaly, high Y/Ho ratios (39–61 with an average of 50) and slightly LREE depletion patterns. Some samples show positive Eu anomalies ($\delta\text{Eu} = 1.02\text{--}1.38$), whereas others show slightly negative Eu anomalies ($\delta\text{Eu} = 0.79\text{--}0.96$). Such REE distribution patterns suggest a dominant seawater origin with subsequent hydrothermal overprints.
- (4) Calcite cements within the cap dolostone give a U–Pb age of $636.5 \pm 7.4/17.8$ Ma (2σ , MSWD = 1.6, $n = 36/40$), which is within uncertainty of a previous dolomite U–Pb age of $629.3 \pm 16.7/22.9$ Ma. These ages suggest Cambrian hydrothermal activity could not have been responsible for the formation of these calcite cements. Instead, they were probably formed during the early Ediacaran period via oxidization of methane clathrates or thermogenic methane oxidation.
- (5) Petrographic, geochronological and geochemical data point to early Ediacaran oxidization of methane clathrates in response to complex interactions between eustasy and isostatic rebound and hydrothermal solutions.

Supplementary material. To view supplementary material for this article, please visit <https://doi.org/10.1017/S001675682200019X>

Acknowledgements. Paul Hoffman and an anonymous reviewer are appreciated for reviewing this manuscript and giving constructive comments. This project was funded by the National Science Foundation of China (grant 41673016 to ZWL), State Key Laboratory of Lithospheric Evolution, Institute of Geology and Geophysics, Chinese Academy of Sciences (grant SKL-Z202001 to ZWL), State Key Laboratory of Palaeobiology and Stratigraphy, Nanjing Institute of Geology and Palaeontology, Chinese Academy of Sciences (grant 193112 to ZWL), and State Key Laboratory of Geological Processes and Mineral Resources, China University of Geosciences (grant GPMR201902 to ZWL).

References

- Baker JA, Peate DW, Waight T and Meyzen C** (2004) Pb isotopic analysis of standards and samples using a ^{207}Pb – ^{204}Pb double spike and thallium to correct for mass bias with a double-focusing MC-ICP-MS. *Chemical Geology* **211**, 275–303.
- Bao HM, Lyons JR and Zhou C** (2008) Triple oxygen isotope evidence for elevated CO_2 levels after a Neoproterozoic glaciation. *Nature* **453**, 504–6.
- Bristow TF, Bonifacie M, Derkowski A, Eiler JM and Grotzinger JP** (2011) A hydrothermal origin for isotopically anomalous cap dolostone cements from south China. *Nature* **474**, 68–71.
- Chew DM, Petrus JA and Kamber BS** (2014) U–Pb LA-ICPMS dating using accessory mineral standards with variable common Pb. *Chemical Geology* **363**, 185–99.
- Condon D, Zhu MY, Bowring S, Wang W, Yang AH and Jin YG** (2005) U–Pb ages from the Neoproterozoic Doushantuo Formation, China. *Science* **308**, 95–8.
- Coogan LA, Parrish RR and Roberts NM** (2016) Early hydrothermal carbon uptake by the upper oceanic crust: insight from in situ U–Pb dating. *Geology* **44**, 147–50.
- Crockford PW, Wing BA, Paytan A, Hodgskiss MSW, Mayfield KK, Hayles JA, Middleton JE, Ahm ASC, Johnston DT, Caxito F, Uhlein G, Halverson GP, Eickmann B, Torres M and Horner TJ** (2019) Barium-isotopic constraints on the origin of post-Marinoan barites. *Earth and Planetary Science Letters* **519**, 234–44.
- Cui H, Orland IJ, Denny A, Kitajima K, Fournelle JH, Baele JM, De Winter NJ, Goderis S, Claeys P and Valley JW** (2019) Ice or fire? Constraining the origin of isotopically anomalous cap carbonate cements by SIMS. *Geological Society of America Abstracts with Programs* **51**. doi: [10.1130/abs/2019AM-332456](https://doi.org/10.1130/abs/2019AM-332456).
- Derkowski A, Bristow TF, Wampler JM, Sřodoń J, Marynowski L, Elliott WC and Chamberlain CP** (2013) Hydrothermal alteration of the Ediacaran Doushantuo Formation in the Yangtze Gorges area (South China). *Geochimica et Cosmochimica Acta* **107**, 279–98.
- Derry LA and Jacobsen SB** (1990) The chemical evolution of Precambrian seawater: evidence from REEs in banded iron formations. *Geochimica et Cosmochimica Acta* **54**, 2965–77.
- Franchi F, Hofmann A, Cavalazzi B, Wilson A and Barbieri R** (2015) Differentiating marine vs hydrothermal processes in Devonian carbonate mounds using rare earth elements (Kess Kess mounds, Anti-Atlas, Morocco). *Chemical Geology* **409**, 69–86.
- Gan T, Luo TY, Pang K, Zhou CM, Zhou GH, Wan B, Li G, Yi QR, Czaja AD and Xiao SH** (2021) Cryptic terrestrial fungus-like fossils of the early Ediacaran Period. *Nature Communications* **12**, 641. doi: [10.1038/s41467-021-20975-1](https://doi.org/10.1038/s41467-021-20975-1).
- Griffin W, Powell W, Pearson NJ and O'Reilly S** (2008) GLITTER: data reduction software for laser ablation ICP-MS. In *Laser Ablation-ICP-MS in the Earth Sciences: Current Practices and Outstanding Issues* (ed. P Sylvester), pp. 308–11. Mineralogical Association of Canada. Short Course Vol. 40.
- Hill CA, Polyak VJ, Asmerom Y and Provencio P** (2016) Constraints on a Late Cretaceous uplift, denudation, and incision of the Grand Canyon region, southwestern Colorado Plateau, USA, from U–Pb dating of lacustrine limestone. *Tectonics* **35**, 896–906.
- Hoffman PF and Schrag DP** (2002) The snowball Earth hypothesis: testing the limits of global change. *Terra Nova* **14**, 129–55.
- Hoffman PF and Macdonald FA** (2010) Sheet-crack cements and early regression in Marinoan (635 Ma) cap dolostones: regional benchmarks of vanishing ice-sheets? *Earth and Planetary Science Letters* **300**, 374–84.
- Horstwood MSA, Kosler J, Gehrels G, Jackson SE, McLean NM, Paton C, Pearson NJ, Sircombe K, Sylvester P, Vermmesch P, Bowring JF, Condon DJ and Schoene B** (2016) Community-derived standards for LA-ICP-MS U–(Th)–Pb geochronology–uncertainty propagation, age interpretation and data reporting. *Geostandards and Geoanalytical Research* **40**, 311–22.
- Hu Y, Feng D, Peckmann J, Roberts HH and Chen D** (2014) New insights into cerium anomalies and mechanisms of trace metal enrichment in authigenic carbonate from hydrocarbon seeps. *Chemical Geology* **381**, 55–66.
- Jiang GQ, Kaufman AJ, Christie-Blick N, Zhang S and Wu H** (2007) Carbon isotope variability across the Ediacaran Yangtze platform in South China: implications for a large surface-to-deep ocean $\delta^{13}\text{C}$ gradient. *Earth and Planetary Science Letters* **261**, 303–20.
- Jiang GQ, Kennedy MJ and Christie-Blick N** (2003) Stable isotopic evidence for methane seeps in Neoproterozoic postglacial cap carbonates. *Nature* **426**, 822–6.
- Jiang GQ, Kennedy MJ, Christie-Blick N, Wu HC and Zhang SH** (2006) Stratigraphy, sedimentary structures, and textures of the late Neoproterozoic Doushantuo cap carbonate in south China. *Journal of Sedimentary Research* **76**, 978–95.

- Jiang GQ, Shi XY, Zhang SH, Wang Y and Xiao SH (2011) Stratigraphy and paleogeography of the Ediacaran Doushantuo Formation (ca. 635–551 Ma) in South China. *Gondwana Research* **19**, 831–49.
- Kalliomäki H, Wagner T, Fusswinkel T and Schultze D (2019) Textural evolution and trace element chemistry of hydrothermal calcites from Archean gold deposits in the Hattu schist belt, eastern Finland: indicators of the ore-forming environment. *Ore Geology Reviews* **112**, 103006. doi: [10.1016/j.oregeorev.2019.103006](https://doi.org/10.1016/j.oregeorev.2019.103006).
- Kamber BS and Webb GE (2001) The geochemistry of Late Archaean microbial carbonate: implications for ocean chemistry and continental erosion history. *Geochimica et Cosmochimica Acta* **65**, 2509–25.
- Kennedy MJ, Christie-Blick N and Sohl LE (2001) Are Proterozoic cap carbonates and isotopic excursions a record of gas hydrate destabilization following Earth's coldest intervals? *Geology* **29**, 443–6.
- Kennedy M, Mrofka D and von der Borch C (2008) Snowball Earth termination by destabilization of equatorial permafrost methane clathrate. *Nature* **453**, 642–5.
- Ku TL, Knauss KG and Mathieu GG (1977) Uranium in open ocean: concentration and isotopic composition. *Deep Sea Research* **24**, 1005–17.
- Lan ZW, Roberts NMW, Zhou Y, Zhang SJ, Li ZS and Zhao TP (2022) Application of *in situ* U–Pb carbonate geochronology to Stenian-Tonian successions of North China. *Precambrian Research* **370**, 106551. doi: [10.1016/j.precamres.2021.106551](https://doi.org/10.1016/j.precamres.2021.106551).
- Lan ZW, Sano Y, Yahagi T, Tanaka K, Shirai K, Papineau D, Sawaki Y, Ohno T, Abe M, Yang HW, Liu H, Jiang T and Wang T (2019) An integrated chemostratigraphic ($\delta^{13}\text{C}$ – $\delta^{18}\text{O}$ – $^{87}\text{Sr}/^{86}\text{Sr}$ – $\delta^{15}\text{N}$) study of the Doushantuo Formation in western Hubei Province, South China. *Precambrian Research* **320**, 232–52.
- Lang XG, Chen JT, Cui H, Man L, Huang KJ, Fu Y, Zhou CM and Shen B (2018) Cyclic cold climate during the Nantuo Glaciation: evidence from the Cryogenian Nantuo Formation in the Yangtze Block, South China. *Precambrian Research* **310**, 243–55.
- Li XH, Li WX, Li ZX, Lo CH, Wang J, Ye MF and Yang YH (2009) Amalgamation between the Yangtze and Cathaysia Blocks in South China: constraints from SHRIMP U–Pb zircon ages, geochemistry and Nd–Hf isotopes of the Shuangxiwu volcanic rocks. *Precambrian Research* **174**, 117–28.
- Li Q, Parrish RR, Horstwood MSA and McArthur JM (2014) U–Pb dating of cements in Mesozoic ammonites. *Chemical Geology* **376**, 76–83.
- Liivamägi S, Šrodoň J, Bojanowski MJ, Gerdes A, Stanek JJ, Williams I and Szczerba M (2018) Paleosols on the Ediacaran basalts of the East European Craton: a unique record of paleoweathering with minimum diagenetic overprint. *Precambrian Research* **316**, 66–82.
- Liivamägi S, Šrodoň J, Bojanowski MJ, Stanek JJ and Roberts NMW (2021) Precambrian paleosols on the Great Unconformity of the East European Craton: an 800 million year record of Baltica's climate conditions. *Precambrian Research* **363**, 106327. doi: [10.1016/j.precamres.2021.106327](https://doi.org/10.1016/j.precamres.2021.106327).
- MacDonald JM, Faithfull JW, Roberts NMW, Davies AJ, Holdsworth CM, Newton M, Williamson S, Boyce A and John CM (2019) Clumped-isotope palaeothermometry and LA-ICPMS U–Pb dating of lava-pile hydrothermal calcite veins. *Contributions to Mineralogy and Petrology* **174**. doi: [10.1007/s00410-019-1599-x](https://doi.org/10.1007/s00410-019-1599-x).
- Meinhold G, Roberts NMW, Arslan A, Jensen S, Ebbestad JOR, Högström AES, Høyberget M, Agić H, Palacios T and Taylor WL (2020) U–Pb dating of calcite in ancient carbonates for age estimates of syn- to post-depositional processes: a case study from the upper Ediacaran strata of Finnmark, Arctic Norway. *Geological Magazine* **157**, 1367–72.
- Michard A (1989) Rare earth element systematics in hydrothermal fluids. *Geochimica et Cosmochimica Acta* **53**, 745–50.
- Nozaki Y, Zhang J and Amakawa H (1997) The fractionation between Y and Ho in the marine environment. *Earth and Planetary Science Letters* **148**, 329–40.
- Nuriel P, Weinberger R, Kylander-Clark ARC, Hacker BR and Craddock JP (2017) The onset of the Dead Sea transform based on calcite age-strain analyses. *Geology* **45**, 587–90.
- Paton C, Hellstrom J, Paul B, Woodhead J and Hergt J (2011) Iolite: freeware for the visualisation and processing of mass spectrometric data. *Journal of Analytical Atomic Spectrometry* **26**, 2508–18.
- Penman DE and Rooney AD (2019) Coupled carbon and silica cycle perturbations during the Marinoan snowball Earth deglaciation. *Geology* **47**, 317–20.
- Petrus JA and Kamber BS (2012) VizualAge: a novel approach to laser ablation ICP-MS U–Pb geochronology data reduction. *Geostandards and Geoanalytical Research* **36**, 247–70.
- Rasbury ET and Cole JM (2009) Directly dating geologic events: U–Pb dating of carbonates. *Review of Geophysics* **47**, 1–27.
- Rasbury ET, Ward WB, Hemming NG, Li H, Dickson JD, Hanson GN and Major RP (2004) Concurrent U–Pb age and seawater $^{87}\text{Sr}/^{86}\text{Sr}$ value of a marine cement. *Earth and Planetary Science Letters* **221**, 355–71.
- Ring U and Gerdes A (2016) Kinematics of the Alpenrhein-Bodensee graben system in the Central Alps: Oligocene/Miocene trans-tension due to formation of the Western Alps arc. *Tectonics* **35**, 1367–91.
- Roberts NMW, Drost K, Horstwood MS, Condon DJ, Chew D, Drake H, Milodowski AE, McLean NM, Smye AJ, Walker RJ and Haslam R (2020) Laser ablation inductively coupled plasma mass spectrometry (LA-ICP-MS) U–Pb carbonate geochronology: strategies, progress, and limitations. *Geochronology* **2**, 33–61.
- Roberts NMW, Rasbury ET, Parrish RR, Smith CJ, Horstwood MSA and Condon DJ (2017) A calcite reference material for LA-ICP-MS U–Pb geochronology. *Geochemistry, Geophysics, Geosystem* **18**, 2807–14.
- Roberts NMW and Walker RJ (2016) U–Pb geochronology of calcite-mineralized faults: absolute timing of rift-related fault events on the northeast Atlantic margin. *Geology* **44**, 531–4.
- Shen GT and Boyle EA (1987) Lead in corals: reconstruction of historical industrial fluxes to the surface ocean. *Earth and Planetary Science Letters* **82**, 289–304.
- Shields GA, Deynoux M, Strauss H, Paquet H and Nahon D (2007) Barite-bearing cap dolostones of the Taoudeni Basin, northwest Africa; sedimentary and isotopic evidence for methane seepage after a Neoproterozoic glaciation. *Precambrian Research* **153**, 209–35.
- Van Kranendonk MJ, Webb GE and Kamber BS (2003) Geological and trace element evidence for a marine sedimentary environment of deposition and biogenicity of 3.45 Ga stromatolitic carbonates in the Pilbara Craton, and support for a reducing Archaean ocean. *Geobiology* **1**, 91–108.
- Vermeech P (2018) IsoplotR: a free and open toolbox for geochronology. *Geoscience Frontiers* **9**, 1479–93.
- Wang JS, Jiang GQ, Xiao SH, Li Q and Wei Q (2008) Carbon isotope evidence for widespread methane seeps in the ca. 635 Ma Doushantuo cap carbonate in south China. *Geology* **36**, 347–50.
- Wang J and Li ZX (2003) History of Neoproterozoic rift basins in South China: implications for Rodinia break-up. *Precambrian Research* **122**, 141–58.
- Woodhead JD and Hergt JM (2001) Strontium, neodymium and lead isotope analyses of NIST glass certified reference materials: SRM 610, 612, 614. *Geostandards Newsletters* **25**, 261–6.
- Wu S, Karius V, Schmidt BC, Simon K and Woerner G (2018) Comparison of ultrafine powder pellet and flux-free fusion glass for bulk analysis of granitoids by laser ablation-inductively coupled plasma-mass spectrometry. *Geostandards and Geoanalytical Research* **42**, 575–91.
- Wu S, Worner G, Jochum KP, Stoll B, Simon K and Kronz A (2019) The preparation and preliminary characterisation of three synthetic andesite reference glass materials (ARM-1, ARM-2, ARM-3) for *in situ* microanalysis. *Geostandards and Geoanalytical Research* **43**, 567–84.
- Wu ST, Yang YH, Jochum KP, Romer RL, Glodny J, Savov IP, Agostini S, De Hoog JCM, Peters STM, Kronz A, Zhang C, Bao ZA, Wang XJ, Li YL, Tang GQ, Feng LJ, Yu HM, Li ZX, Zhang L, Lin J, Zeng Y, Xu CX, Wang YP, Cui Z, Deng L, Xiao J, Liu YH, Xue DS, Zhang D, Jia LH, Wang H, Xu L, Huang C, Xie LW, Pack A, Woerner G, He MY, Li CF, Yuan HL, Huang F, Li QL, Yang JH, Li XH and Wu FY (2021) Isotopic compositions (Li–B–Si–O–Mg–Sr–Nd–Hf–Pb) and $\text{Fe}^{2+}/\Sigma\text{Fe}$ ratios of three synthetic andesite glass reference materials (ARM-1, ARM-2, ARM-3). *Geostandards and Geoanalytical Research* **45**, 719–45.
- Wu ST, Yang YH, Wang H, Huang C, Xie LW and Yang JH (2020a) Characteristic performance of guard electrode in LA-SF-ICP-MS for multi-element quantification. *Atomic Spectroscopy* **41**, 154–61.
- Wu ST, Yang M, Yang YH, Xie LW, Huang C, Wang H and Yang JH (2020b) Improved *in situ* zircon U–Pb dating at high spatial resolution (5–16 μm) by

- laser ablation–single collector–sector field–ICP–MS using Jet sample and X skimmer cones. *International Journal of Mass Spectrometry* **456**, 116394. doi: [10.1016/j.ijms.2020.116394](https://doi.org/10.1016/j.ijms.2020.116394).
- Wu ST, Yang YH, Roberts NMW, Yang M, Wang H, Lan ZW, Xie BH, Li TY, Xu L, Huang C, Xie LW, Yang JH and Wu FY** (2022) In situ calcite U–Pb geochronology by high-sensitivity single-collector LA-SF-ICP-MS. *Science China Earth Sciences*, doi: [10.1007/s11430-021-9907-1](https://doi.org/10.1007/s11430-021-9907-1).
- Yang C, Rooney AD, Condon DJ, Li XH, Grazhdankin DV, Bowyer FT, Hu CL, Macdonald FA and Zhu MY** (2021) The tempo of Ediacaran evolution. *Science Advances* **7**, eabi9643. doi: [10.1126/sciadv.abi9643](https://doi.org/10.1126/sciadv.abi9643).
- Zhou CM, Bao HM, Peng YB and Yuan XL** (2010) Timing the deposition of ¹⁷O-depleted barite at the aftermath of Nantuo glacial meltdown in South China. *Geology* **38**, 903–6.
- Zhou GH, Luo TY, Zhou MZ, Xing LC and Gan T** (2017) A ubiquitous hydrothermal episode recorded in the sheet-crack cements of a Marinoan cap dolostone of South China: implication for the origin of the extremely ¹³C-depleted calcite cement. *Journal of Asian Earth Sciences* **134**, 63–71.